Chemistry
A European
Journal

Chemistry Europe
European Chemical Societies Publishing

Accepted Article

Title: Fe(II) metallohelices stabilize DNA G-quadruplexes and down-regulate expression of G-quadruplex regulated oncogenes

Authors: Jaroslav Malina, Hana Kostrhunova, Peter Scott, and Viktor Brabec

To be cited as: *Chem. Eur. J.* 10.1002/chem.202101388

Link to VoR: https://doi.org/10.1002/chem.202101388

WILEY-VCH

10.1002/chem.202101388

WILEY-VCH

FULL PAPER

Fe(II) Metallohelices Stabilize DNA G-Quadruplexes and Down-regulate Expression of G-Quadruplex Regulated Oncogenes

Jaroslav Malina,[a] Hana Kostrhunova,[a] Peter Scott,[b] and Viktor Brabec*[a]

Abstract: DNA G-quadruplexes (G4s) were identified within the promoter regions of many proto-oncogenes. Thus, G4s represent attractive targets for cancer therapy and the design and development of new drugs as G4 binders is a very active field of medicinal chemistry. Here, we employed methods of molecular biophysics and biology to investigate the interaction of chiral metallohelices with a series of four DNA G4s (*hTelo*, *c-myc*, *c-kit1*, *c-kit2*) that are formed by the human telomeric sequence (*hTelo*) and in the promoter regions of *c-MYC* and *c-KIT* proto-oncogenes. We show that the investigated water-compatible optically pure metallohelices made by self-assembly of simple nonpeptidic organic components around Fe(II) ions, which exhibit bioactivity emulating the natural systems, bind with high affinity to G4 DNA and much lower affinity towards duplex DNA. Notably, both enantiomers of metallohelix containing *m*-xylenyl bridge (**5b**) were found to be effective inhibitors of primer elongation catalyzed by *Taq* DNA polymerase by stabilizing G4 structures formed in the template strands containing *c-myc* and *c-kit2* G4-forming sequences. Moreover, both enantiomers of **5b** down-regulated the expression of *c-MYC* and *c-KIT* oncogenes in human embryonic kidney cells at mRNA and protein levels. As metallohelices also bind alternative nucleic acid structures, they hold promise as potential multi-targeted drugs.

Introduction

Prostate DNA G-quadruplexes (G4s) are highly stable tetra-stranded secondary structures formed by stacking of G-quartets (i.e., interaction of four guanines linked by Hoogsteen hydrogen bonding). These structures are further stabilized by monovalent cations (e.g., Na^+, K^+) that occupy the central cavities between the stacks and neutralize the electrostatic repulsion. G4s can display a wide range of topologies depending on the relative orientation of the strands and on the length and nucleotide composition of loops connecting the G-rich sequences.[1] DNA G4s were detected in human cells, primarily in telomeres and in genomic DNA.[2] High-throughput sequencing detected more than 700 000 sequences in the human genome that can fold into G4 structures.[3] The discovery of the relationship between maintaining telomeres and tumor progression sparked great interest in studying telomere G4s, telomere-specific proteins, and telomerases and their potential for cancer therapy.[4] G4s were identified within the promoter regions of many proto-oncogenes, such as BCL2,[5] RET,[6] KRAS,[7] VEGF,[8] PDGF-A,[9] *c-MYC*,[10] or *c-KIT*,[11] suggesting that G4s play a role in cancer growth and progression. As an example, proto-oncogenes of the *MYC* family are upregulated in >70% of human cancers,[12] and ligand-induced stabilization of G4 in the promoter region has been shown to prevent the expression of *c-MYC*.[13] Another example, *c-kit* proto-oncogene, associated with several types of cancer and the main cause of gastrointestinal cancer,[14] contains two G4 forming sequences in its promoter region, and stabilization of these G4 structures correlates with the down-regulation of *c-KIT* gene expression.[15]

It is therefore not surprising that G4s represent attractive targets for anticancer therapy, and to date, according to the G4 ligands database (http://www.g4ldb.org),[16] around 1000 small molecules capable of stabilizing G4s have been reported. Such synthetic G4 binders typically contain planar aromatic chromophores for π-π stacking with G-tetrads, positively charged side chains for binding to loops and grooves of the G4, and steric bulk to prevent intercalation between DNA base pairs.[1, 17]

Reports of non-planar molecules interacting with G4s are quite scarce,[18] although in contrast many natural proteins have been identified that interact with G4s,[19] commonly via α-helical recognition units.[20] In this context we note that certain metallo-supramolecular helical assemblies, which have similar size, shape, charge, and amphipathic architectures to short cationic α-helical peptides[21] have been shown also to interact. Qu and co-workers reported that chiral metallo-supramolecular helicates ($[\mathbf{M}_2\mathbf{L}_3]^{4+}$; **M** = Ni(II) or Fe(II); **L** = $C_{25}H_{20}N_4$) are able to selectively stabilize human telomeric DNA G4 and inhibit telomerase activity.[22] Enantioselective stabilization of human telomeric G4 and inhibitory effect on telomerase was demonstrated for a chiral Fe(II) based metallohelical complex **5a** (Figure 1A).[23] This compound, developed in one of our laboratories, was the prototype for several classes of self-assembling, optically pure, water-stable metallohelices based on helical arrays of fully-encapsulated Fe ions connected by different linking bridges (e.g. Figure 1)[24] We first reported that **5a** exhibits promising antimicrobial activity[24] and that it can bind to DNA and stabilize DNA junctions and bulges.[25] **5a** was used as a prototype compound for the development of a new class of metallohelices **5b**-**h** (Figure 1) that showed structure-dependent activity against Gram-positive and –negative bacteria.[26] We have recently reported that metallohelices accumulate in eukaryotic cells and in the cell nucleus, allowing them to interact with nuclear DNA.[27] Metallohelices were able to condense/aggregate DNA and inhibit *in vitro* DNA-related enzymatic activities such as transcription and DNA relaxation by topoisomerase I.[26-27]

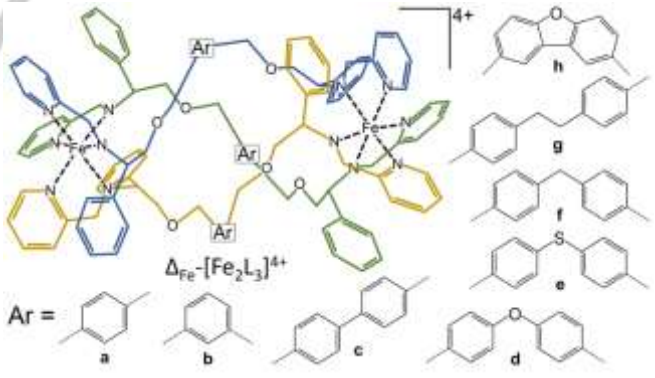

Figure 1. Enantiomerically pure Fe(II) metallohelices **5a**-**h**.

[a] Dr. J. Malina, Dr. H. Kostrhunova, Prof. Dr. V. Brabec
Czech Academy of Sciences, Institute of Biophysics, Kralovopolska 135, CZ-61265 Brno, Czech Republic
E-mail: brabec@ibp.cz
[b] Prof. P.Scott
Department of Chemistry, Unoversity of Warwick
Coventry, CV4 7AL, UK
Supporting information for this article is available on the WWW under https://doi.org/…..

In the present work, we employed fluorescence intercalator displacement (FID) assays, fluorescence resonance energy transfer (FRET) melting assays, 2-aminopurine fluorescence-based binding studies, and DNA polymerase stop assays to investigate the interaction of the Λ- and Δ-enantiomers of **5a**-**h** (Figure 1) [26] with a series of four DNA G4s (*hTelo*, *c-myc*, *c-kit1*, *c-kit2*) that are formed by the human telomeric sequence (*hTelo*) and in the promoter regions of *c-MYC* and *c-KIT* proto-oncogenes. The downstream effect of **5b** has been explored in human embryonic kidney cells using real-time quantitative PCR and Western blotting.

Results

Fluorescence intercalator displacement (FID) assay

The affinity of metallohelices towards DNA G4s (*hTelo*, *c-myc*, *c-kit1*, *c-kit2*) and a control duplex DNA (26_ds) was initially evaluated by using the FID assay.[28] Selected G4s differ by topology and by nucleotide composition and length of intervening loops. The human telomeric G4 (*hTelo*) adopts a basket-type antiparallel arrangement[29] while *c-myc*, *c-kit1*, and *c-kit2* G4s fold into the parallel topology. The CD spectra of folded oligonucleotides in the absence of metallohelices (Figure S1 in the Supporting information) are consistent with the predicted topologies.[29-30]

DNA strands were preincubated with thiazole orange (TO) and then titrated with metallohelices while monitoring the fluorescence of TO. The DC_{50} values correspond to a 50% decrease in dye fluorescence (see plots in Figure S2 in the Supporting information), which is a good indicator of the ability of a studied ligand to interact with a DNA structure. Ligands with DC_{50} values equal to or lower than 0.5 μM are regarded as excellent G4 binders.[28] The DC_{50} values obtained in 40 mM K^+ are graphically presented in Figure 2 (for numerical values, see Table S1 in the Supporting information) and show that **5a**-**h** possess a higher affinity towards DNA G4s and lower affinity towards duplex DNA. The highest and lowest binding affinities were observed for *c-myc* (DC_{50} values between 0.23 and 0.48 μM) and *c-kit1* (DC_{50} values between 0.47 and 0.75 μM) G4s, respectively. The DC_{50} values obtained for the binding of metallohelices to duplex DNA were in the range from 0.66 to 2.91 μM.

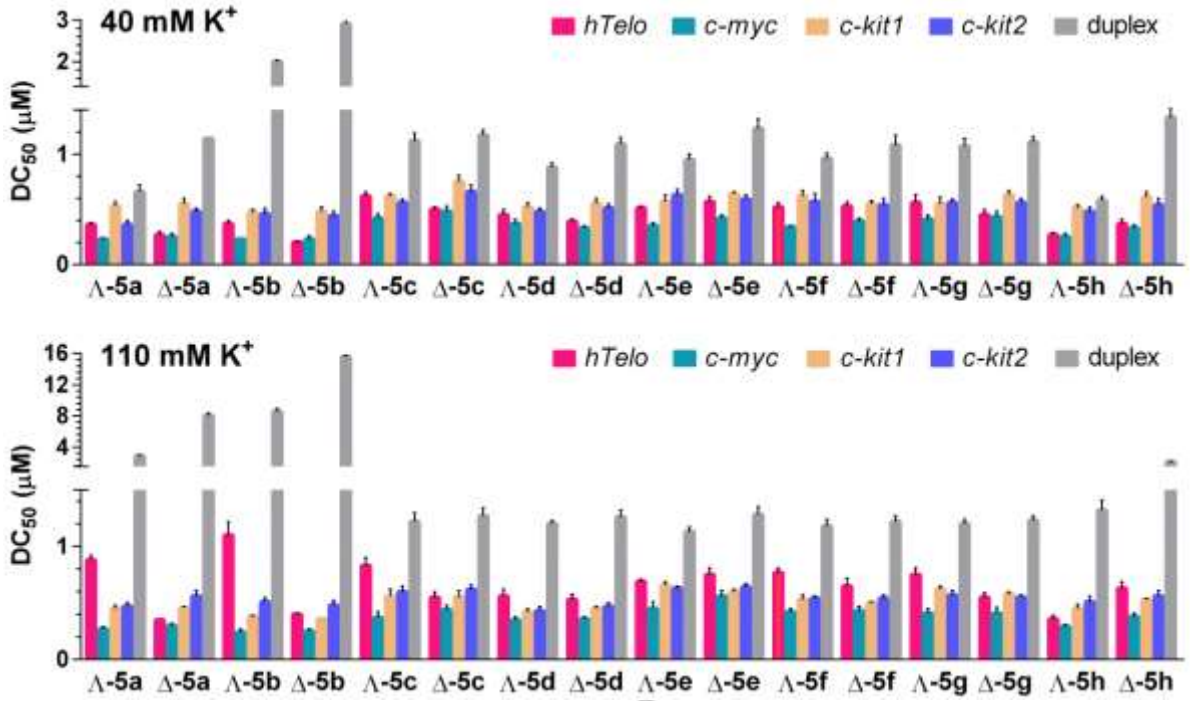

Figure 2. DC_{50} values (μM) for DNA G4s and a short DNA duplex determined by FID upon addition of the metallohelices in 10 mM potassium phosphate buffer (pH 7) and the presence of 30 mM (upper panel) and 100 mM (lower panel) KCl. The results are expressed as mean ± SD from 2 independent experiments

Selectivity indexes calculated as the ratio of the DC_{50} values determined for the DNA duplex and G4 are displayed in Figure 3 (for numerical values, see Table S2 in the Supporting information), and as can be seen, both enantiomers of **5b** outperform the remaining metallohelices in binding selectivity to G4s. The highest selectivity indexes of 14.6 and 13 were observed for the binding of **Δ-5b** to *hTelo* and *c-myc* G4s, respectively.

FID assays were repeated in the presence of 110 mM K^+ to probe the effect of ionic strength on the binding affinity of metallohelices carrying a high positive charge of 4+. The DC_{50} values summarized in Figure 2, and Table S3 in the Supporting information show that the effect of high ionic strength on the binding affinity of **5a**-**h** depends on the type of G4 and differs among metallohelices. A lowering of the binding strength was observed for *hTelo*, *c-myc*, and *c-kit2* G4s, while the binding of metallohelices to *c-kit1* G4 was slightly enhanced (i.e., DC_{50} values were lowered).

The most weakened by the heightened concentration of K^+ was the binding of Λ-**5a** and both enantiomers of **5b** to *hTelo* G4. Inspection of data in Figure 2 reveals that binding affinities of metallohelices to duplex DNA were in most cases reduced. While the DC_{50} values of **5c**-**g** for duplex DNA were slightly increased, the DC_{50} values of **5a**, **5b**, and **5h** were incremented several-fold, and so were the values of the selectivity index (see Figure 3 and Table S4 in the Supporting information). The Δ-**5b** displayed the highest selectivity index values of 33, 39, 43, and 62 for *c-kit2*, *hTelo*, *c-kit1*, and *c-myc* G4s, respectively.

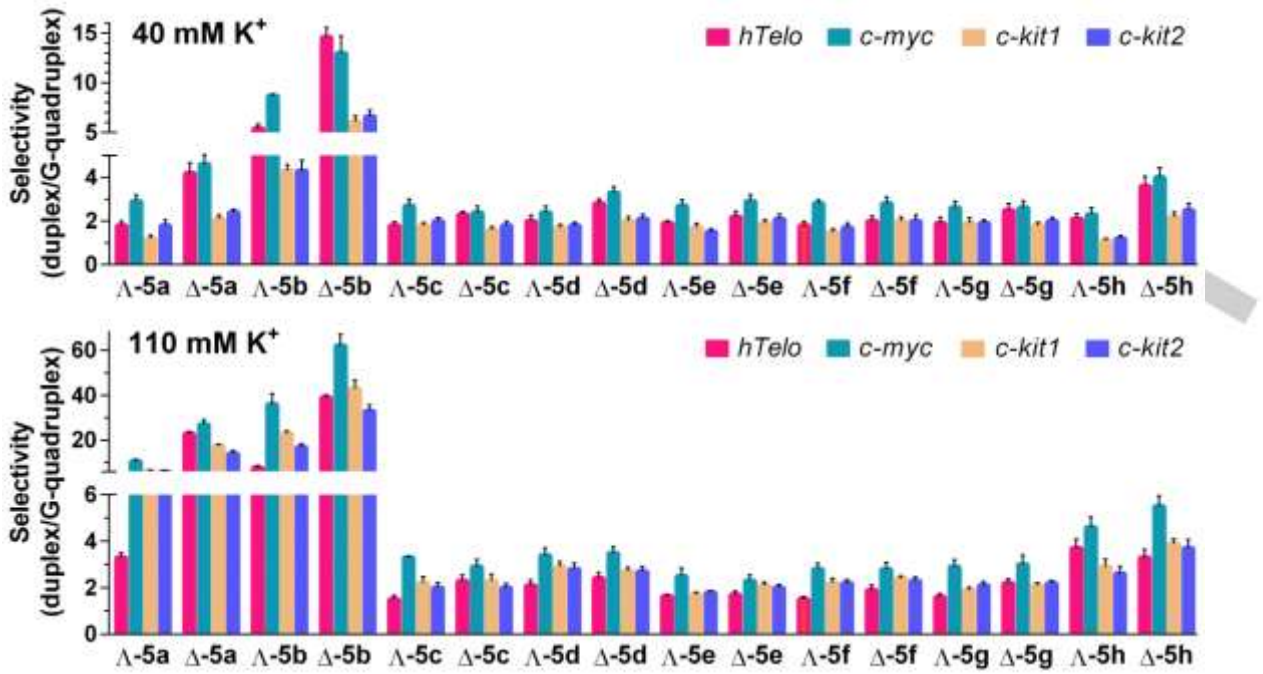

Figure 3. Selectivity indexes of metallohelices towards DNA G4s in 10 mM potassium phosphate buffer (pH 7) and the presence of 30 mM (upper panel) and 100 mM (lower panel) KCl. The values of the binding selectivity for each metallohelix were calculated as a ratio between the DC_{50} values obtained for the DNA duplex and G4. The results are expressed as mean ± SD from two independent experiments.

These results indicate that the binding of metallohelices to *hTelo* G4 is more dependent on electrostatic interactions than the binding to *c-myc*, *c-kit1*, and *c-kit2* G4s and that electrostatic interactions are particularly important for the binding of **5a** a **5b** to duplex DNA.

Notably, the selectivity indexes (SIs) of **Δ-5a**, **Λ-5b**, and **Δ-5b** in 110 mM K^+ are comparable to those of some high-affinity G4 binders such as **360A** (SI = 35.7 in 100 mM K^+ towards *hTelo*) or **Phen-DC$_3$** (SI = 35.7 in 100 mM K^+ towards *hTelo*).[31] On the other hand, the well-documented G4 binder **TmPyP4** that was shown *in vitro* to inhibit c-*MYC* transcription[10] is known to be poorly selective (SI = 1.8 in 100 mM K^+ towards *hTelo*).[28]

FRET melting assay

The potency of metallohelices to stabilize DNA G4s was investigated by the FRET melting assay. This method is based on the monitoring of melting profiles of G4-forming oligonucleotides labeled with FRET fluorophores[32] and allows the determination of the G4 thermal stability in the presence of non-labeled competing DNA.

The fluorescently labeled G4s at the concentration of 0.4 μM were mixed with 0.4 μM **5a**-**h** in the absence and in the presence of increasing concentrations (60-240 μM, concentration per nucleotide) of double-stranded (ds) DNA from *Micrococcus luteus* and their melting temperature (T_m) was determined with the aid of a real-time PCR cycler (see examples of the melting curves in Figures S3-S6 in the Supporting information). Figure S3 shows that the melting profile of *hTelo* G4, unlike melting profiles of *c-myc*, *c-kit1*, and *c-kit2* (Figures S4-S6), changed its shape upon addition of **5a**-**h** from monophasic to biphasic. The biphasic melting suggests either the presence of two structures with two different T_m values or a metallohelix-induced conformational change of the G4 structure that melts in two steps. *hTelo* is polymorphic and a change in its topology due to the binding of metallohelices may be responsible for the biphasic FRET melting. Since the ΔT_m values for the first melting transition in the presence of metallohelices oscillated around zero, the ΔT_m values for *hTelo* G4 were calculated from the second melting transition.

The ΔT_m values presented in Figure 4 show that **5a**-**h** at 1:1 (metallohelix:G4) ratio markedly enhanced the thermal stability of all tested G4s and were able to stabilize G4s even in excess of competing dsDNA. In these experiments, a reduced concentration of K^+ was used, as the melting point of *c-myc* and *c-kit2* in 40 mM K^+ was 87 °C and 77 °C, which complicated / prevented the evaluation of the stabilizing abilities of the helicates. Nevertheless, the results shown in Figure 4 imply enhanced binding preference of **5a**-**h** to G4 DNA over dsDNA. Consistent with the previous results, the most potent stabilizers of G4s were the enantiomers of **5b**. The exception was the stabilization of *c-myc* G4, where the Λ-**5b** was considerably less active than Δ-**5b** and the enantiomers of **5a**, **5c**, and **5h**. The thermal stability of duplex DNA (26_ds) in the presence of **5a**-**h** was also probed using the same experimental conditions, and examples of the melting curves are displayed in Figure S7 in the Supporting Information. The stabilizing effect of metallohelices on 26_ds in the absence of dsDNA was weak ($\Delta T_m \leq 1$ ºC) and disappeared completely upon the addition of 60 μM dsDNA.

Closer inspection of data in Figure 4 reveals that some ΔT_m values are not perfectly consistent with the FID data. This discrepancy could be at least partly explained by the differences in experimental conditions between FRET and FID assays. It must also be taken into consideration that the melting temperatures of individual G4s significantly differ, which makes direct comparison of the thermal stabilization capacities of **5a**-**h** among different G4s impossible. The T_m values for *hTelo*, *c-myc*, *c-kit1*, and *c-kit2* G4s in the absence of metallohelices were 45.5 ºC, 71.6 ºC, 46.8 ºC, and 63.2 ºC, respectively. A further possible reason is that the FID assay has been validated using a set of known and fully characterized G4-binding ligands, and in most cases, FID results were in good agreement with the FRET data.[28] Nevertheless, some ligands with

10.1002/chem.202101388

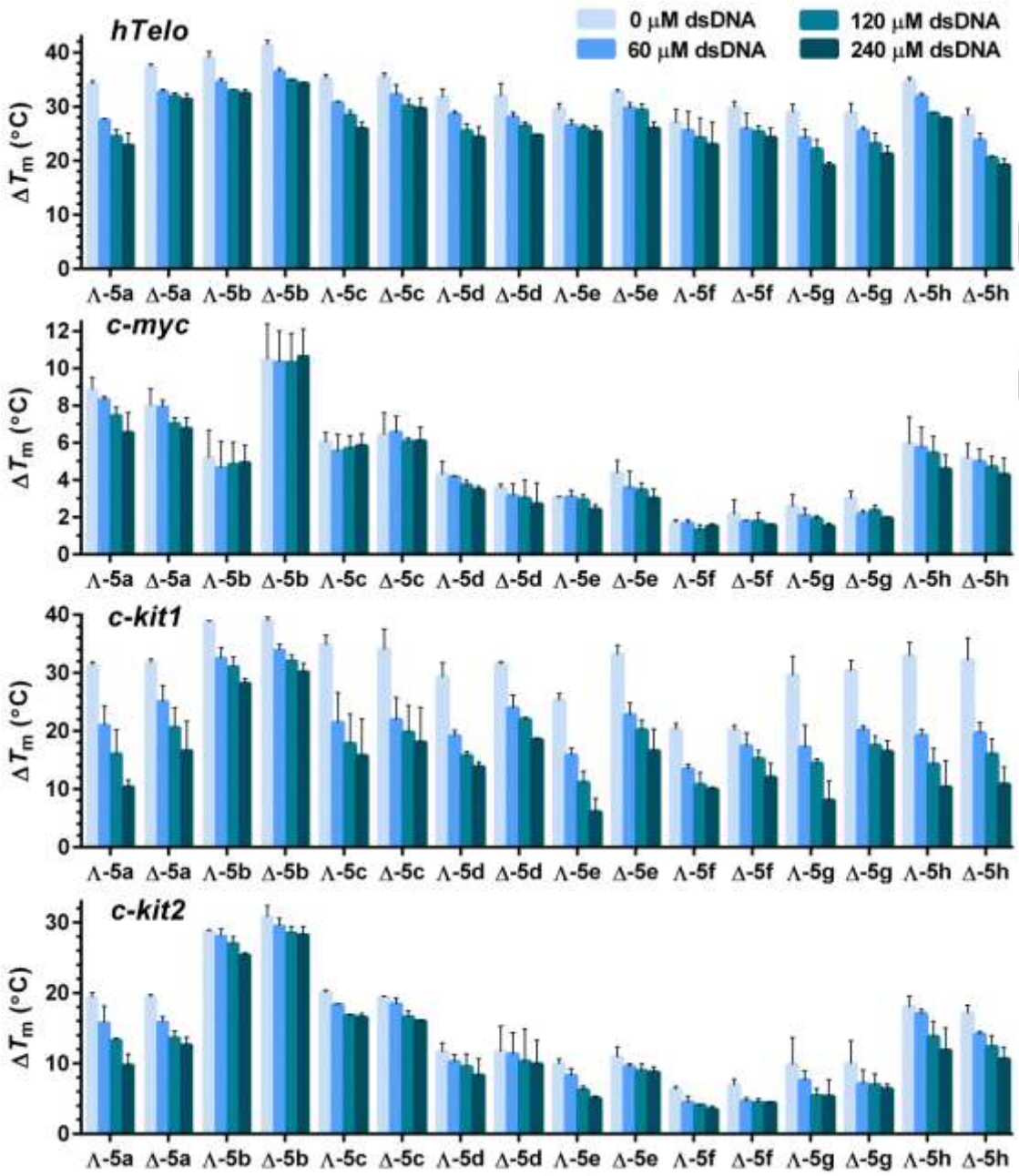

Figure 4. ΔT_m values for the fluorescent-labeled *hTelo*, *c-myc*, *c-kit1*, and *c-kit2* DNA G4s (0.4 μM) determined by FRET upon addition of 0.4 μM **5a**-**g** in the absence and in the presence of increasing concentrations (indicated in the Figure) of dsDNA. The results are expressed as mean ± SD from three independent experiments. The buffer conditions were 4 mM potassium phosphate (pH 7).

low DC_{50} values exhibited unexpectedly low thermal stabilizations. The discrepancy comes from different binding modes of the ligands. Whereas planar ligands that stack on one G-tetrad displace TO by direct competition, compounds susceptible to establish additional interactions with loops or grooves might displace TO by both direct and indirect competition (i.e., binding to a nearby site). It means that the FID and FRET assays represent complementary methods that differ in the relative weights of the π-stacking and the electrostatic contributions. This should be taken into account when comparing data obtained by using these two methods for such structurally complex and highly charged compounds as metallohelices.

2-aminopurine fluorescence studies

In an effort to gain information on the binding mode of metallohelices to G4s, we employed 2-aminopurine (2Ap), a fluorescent isomer of adenine, that was incorporated into the loops of *hTelo* G4. This approach has been previously used to probe the binding of TMPyP4 [33] and metallo-supramolecular helicate ($[M_2L_3]^{4+}$; M = Ni(II) or Fe(II); L = $C_{25}H_{20}N_4$)[22a] to *hTelo*. The 2Ap replaced adenine in the TTA loops in positions 7, 13, and 19 (see scheme in Figure 5A) in order to monitor the interaction between **5a**-**g** and *hTelo* G4. Complex **5h** was omitted from the 2Ap fluorescence study, because its intrinsic fluorescence overlaps with that of 2Ap. The fluorescence of 2Ap is strongly quenched by adjacent bases within the structure of dsDNA but is enhanced when the base stacking or base pairing is perturbed.

10.1002/chem.202101388

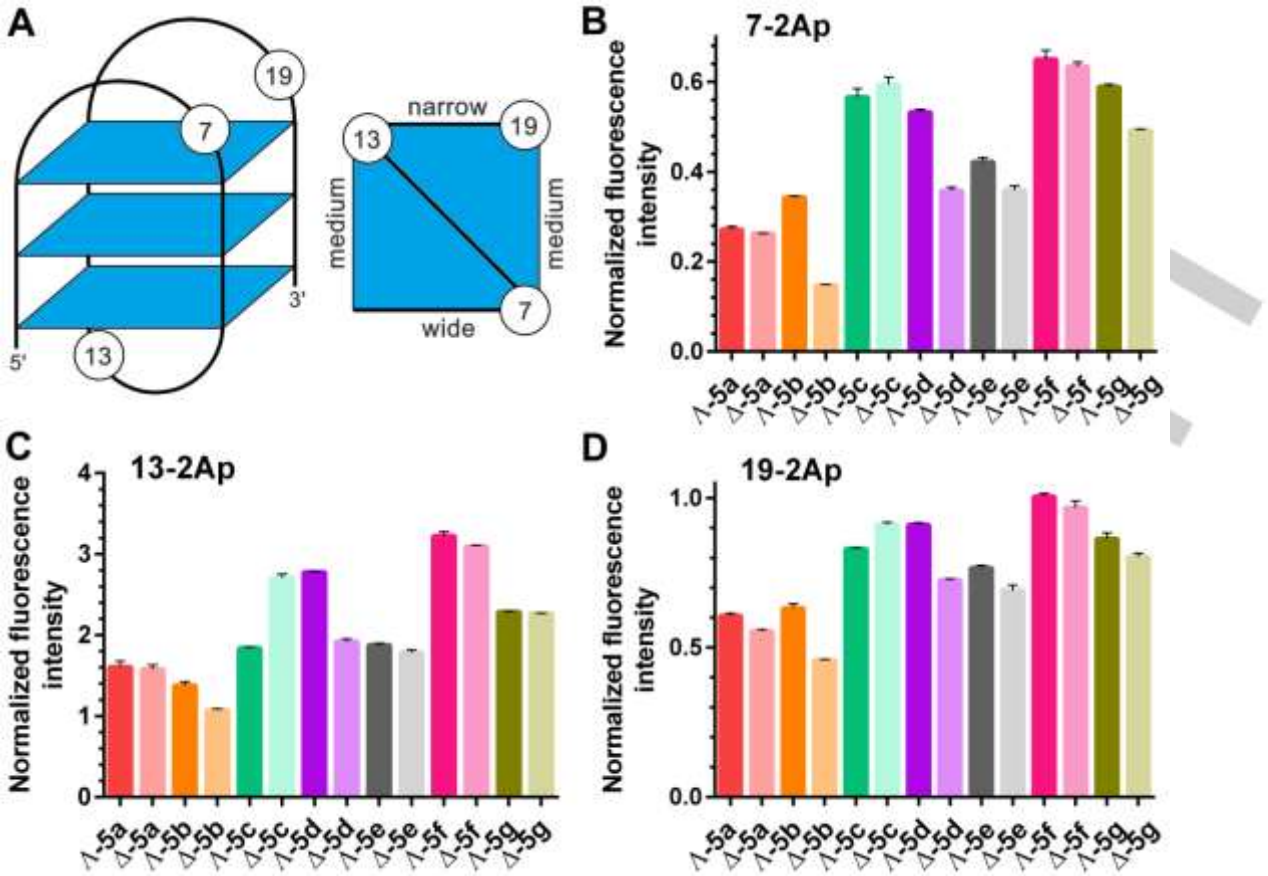

Figure 5. (A) Scheme of *hTelo* G4 with numbers corresponding to the positions of 2Aps and a top view showing positions of 2Aps and groove widths. (B-D) Influence of metallohelices (8 μM) on the fluorescence of *hTelo* (4 μM) labeled with 2Aps at positions 7 (B), 13 (C), and 19 (D). The results are expressed as mean ± SD from 2 independent experiments.The buffer conditions were 10 mM potassium phosphate (pH 7) and 30 mM KCl.

Other factors known to affect the fluorescence of 2Ap are collisions with other bases and biomolecular interactions.[34] Because the π-stacking within the TTA loops in a G4 is highly distorted, the electron transfer quenching of 2Ap by adjacent bases is less efficient. The **5a-g** were mixed with the 2Ap-labeled G4 at 2:1 (metallohelix:G4) ratio, and the intensity of 2Ap fluorescence was recorded. The 2:1 ratio was selected in the preliminary titration experiments (see Figure S8 in the Supporting information). The results in Figure 5B-D show that the fluorescence intensity of 2Ap is significantly affected in the presence of **5a-g,** indicating a strong interaction between metallohelices and the G4. As can be seen, **5a-g** induced a strong reduction of 2Ap fluorescence in position 7, a slight reduction of 2Ap fluorescence in position 19, and a substantial increase of 2Ap fluorescence in the diagonal loop in position 13. The 3-fold enhancement of the fluorescence intensity of 2Ap at position 13 has been registered for the interaction of *hTelo* with TMPyP4,[33] which is known to insert between a central diagonal loop and the adjacent G-quartet.[35] Such binding mode is, however, unlikely for metallohelices because of their size and cylindrical shape.

The reduction of the fluorescence intensity of 7-2Ap and 19-2Ap might suggest that metallohelices stack to the G-quartet between the lateral loops where they could be in close contact with both 2Aps. Another possibility is the binding of metallohelices to the medium groove formed between strands containing 7-2Ap and 19-2Ap. In both cases, a conformational change of the G4 structure induced by a metallohelix could lead to the flipping-out of 13-2Ap from the diagonal loop and enhancement of its fluorescence.

The presence of **5a** and **5b** resulted in a stronger reduction of 2Ap fluorescence at positions 7 and 19 than it was registered for **5c-h,** which is in agreement with the higher binding affinity of **5a** and **5b** to *hTelo* G4 as it was detected by the FID assay. The unexpectedly high intensity of 2Ap fluorescence that was recorded for the binding of **5h** results from the intrinsic fluorescence of **5h** that overlaps with the fluorescence of 2Ap.

DNA polymerase stop assay

The stabilizing activity of **5a** and **5b** towards *hTelo*, *c-myc*, *c-kit1*, and *c-kit2* G4s was further explored using a *Taq* DNA polymerase stop assay that is widely used to demonstrate the ligand-induced stabilization of G4s formed in the template strand.[36]

Figure 6 and Figure S9 in the Supporting information show the results of *Taq* DNA polymerase primer extension reactions on DNA templates containing *hTelo*, *c-myc*, *c-kit1*, and *c-kit2* G4-forming sequences in the presence of increasing concentrations of Λ- and Δ-enantiomers of **5a** and **5b**. It can be seen that in the absence of the metallohelices, there was only slight pausing of the DNA polymerase when it reached the G-rich site. However, the addition of **5a** and **5b** resulted in an enhancement of pausing at the same site as that observed in the absence of metallohelices. Two bands for the pausing site observed in Figure 6A in the case of *c-kit1* was apparently a consequence of the gradual unwinding of the *c-kit1* structure during the process when DNA polymerase overcomes the G-quadruplex

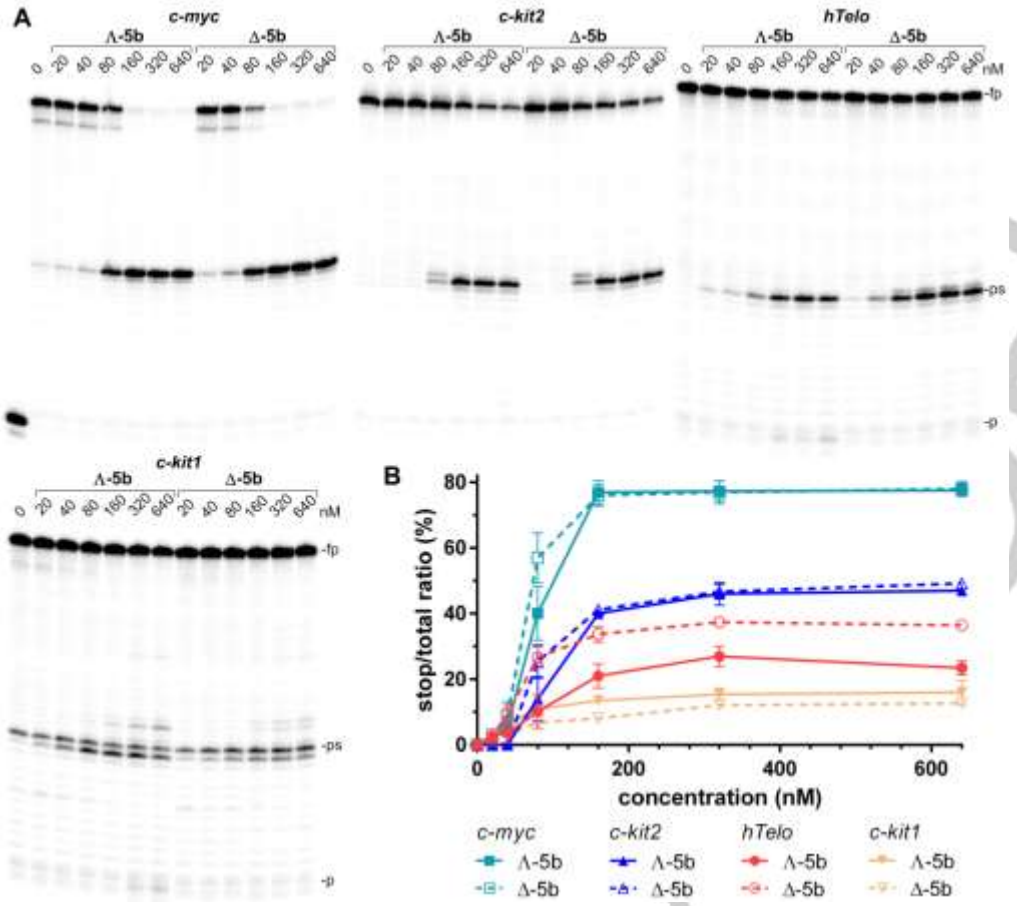

Figure 6. Inhibition of *Taq* polymerase DNA synthesis across template (30 nM) containing *c-myc*, *c-kit2*, *c-kit1*, and *hTelo* G4 forming sequences in the presence of increasing concentrations of **5b**. (A) Autoradiograms of 12% PAA sequencing gels with products of DNA synthesis on the templates containing *c-myc*, *c-kit2*, *c-kit1,* and *hTelo* G4 forming sequences in the presence of Λ- and Δ-enantiomers of **5b**. *fp*, *ps*, and *p* correspond to full-length product, pausing site by G4, and primer, respectively. (B) Plots showing the ratio of the radiation corresponding to pausing sites to total radiation of the lane *vs.* concentrations of Λ- and Δ-enantiomers of **5b**. The results are expressed as mean ± SD from two independent experiments.

barrier. This conclusion is supported by the results shown in Figure 6B demonstrating that *c-kit1* was the least effective in arresting DNA polymerase. The results shown in Figure 6A suggest that both metallohelices increase the polymerase pausing by stabilizing the G4 structure. The results were quantified as the percentage of normalized stop product with respect to the total intensity per lane. Inspection of plots in Figures 6B and S9B reveals that **5b** exhibits slightly increased potency to stabilize G4s and halt DNA polymerase than **5a** and that both compounds were particularly effective in stopping DNA polymerase on the template containing *c- myc* G4-forming sequence. **5b** was capable of inducing the formation of strong stop sites on the *c-myc* template at a concentration as low as 80 nM (Figure 6A). **5a** and **5b** were less efficient in inhibiting the primer elongation on the templates containing *c-kit2* and *hTelo* G4-forming sequences, and the lowest inhibitory effect was observed for the template with *c-kit1* G4 sequence.

The differences between Λ- and Δ-enantiomers of **5a** and **5b** on *c-myc*, *c-kit1*, and *c-kit2* templates were relatively low, although the inhibiting activity of the Δ-enantiomer appeared to be slightly higher. On the other hand, the Δ-enantiomers of **5a** and **5b** were markedly more active than the Λ-enantiomers in blocking *Taq* DNA polymerase on the template capable of *hTelo* G4 formation, which is in agreement with the FID results.

To further demonstrate that the inhibition of DNA synthesis was a result of a metallohelix-induced G4 stabilization, additional experiments were carried out using *c-myc* and *c-kit2* control templates containing mutated sequences that cannot fold into G4s because the middle guanines in GGG sequences participating in the formation of G4s were replaced by cytosines (see their sequences in the Experimental section). Gels in Figure S10 in the Supporting information show that **5b** did not inhibit DNA synthesis on templates with mutated sequences. It implies that the inhibition of DNA polymerization by metallohelices does result from the stabilization of G4 structures formed in the template strands.

Down-regulation of *c-MYC* and *c-KIT* proto-oncogenes in human cells

Since the previous experiments identified **5b** as the most promising G4 binder of the tested metallohelices, the inhibitory effect of **5b** on the expression of *c-MYC* and *c-KIT* genes in human embryonic kidney cells HEK 293 was evaluated.

First, the capability of **5b** enantiomers to inhibit the growth of HEK 293 cells was determined. Cells were exposed to increasing concentrations of Λ-**5b** and Δ-**5b** for 72h, which resulted in a concentration-dependent inhibition of cell growth, with IC_{50} values 5.0 ± 0.9 and 14.6 ± 2.2 μM for Λ-**5b** and Δ-**5b**, respectively.

The impact of **5b** enantiomers on *c-MYC* and *c-KIT* transcription in HEK 293 cells was then explored by monitoring the mRNA expression using qRT-PCR (Figure 7A, B). Λ-**5b** and Δ-**5b** were

10.1002/chem.202101388

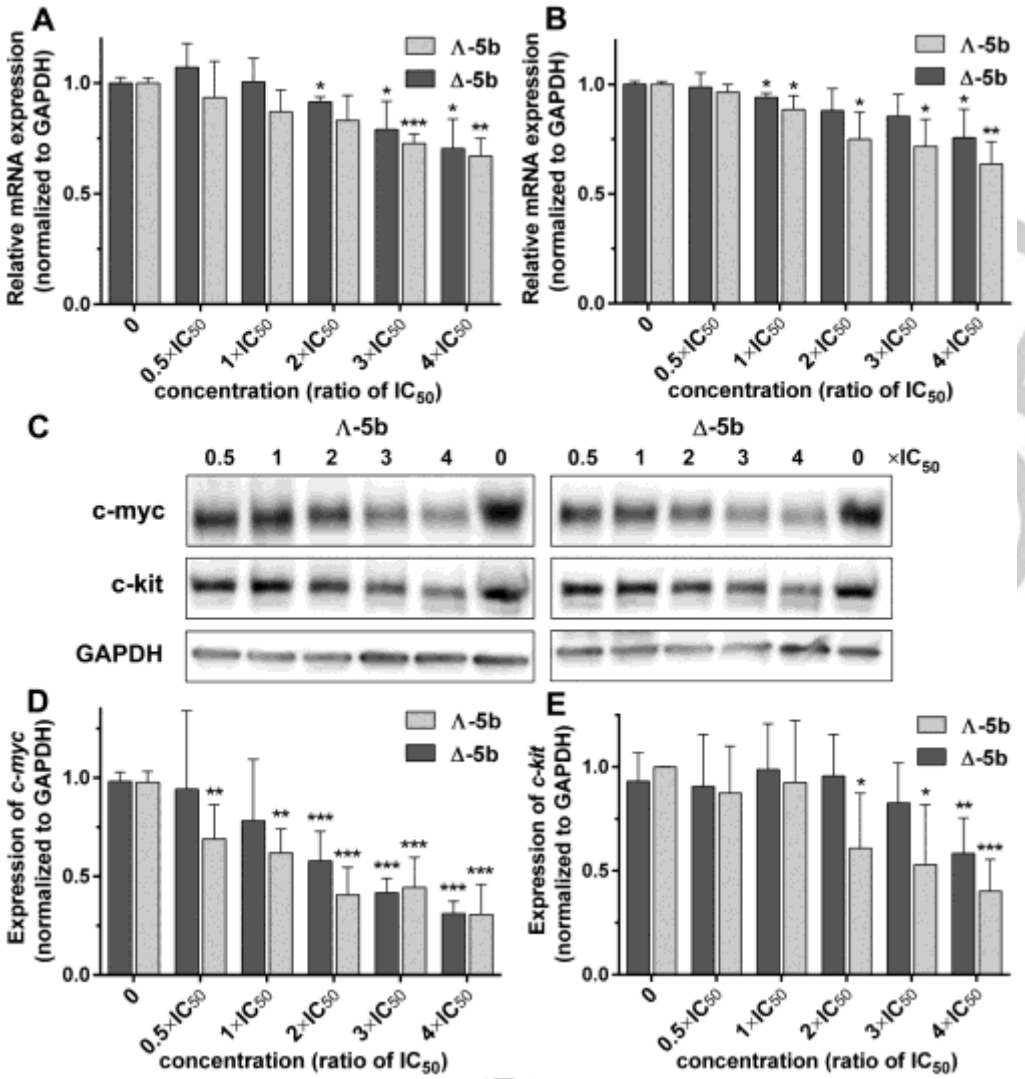

Figure 7. Down-regulation of *c-MYC* (A) and *c-KIT* (B) mRNA in HEK 293 cells treated with Λ-**5b** and Δ-**5b**. RNA isolated from cells after 24 h treatment with the indicated concentrations of **5b** was reverse transcribed, and qRT-PCR was performed. Data is presented in terms of fold change. Normalization was done with respect to the GAPDH gene. Three independent sets of samples, each in triplicate were evaluated (averages of the replicates were analyzed; n=3). Data are shown as mean ±SD. *p ≤ 0.05; **p ≤ 0.01; ***p ≤ 0.001. (C-E) Decrease of c-myc and c-kit protein levels in HEK 293 cells treated with Λ-**5b** and Δ-**5b**. (C) Western blot analysis of *c-MYC* and *c-KIT* expression in cells treated for 24 h with the indicated concentrations of **5b**, representative images. Quantification of c-myc (D) and c-kit (E) protein expression normalized to GAPDH. Data are presented in terms of fold change. Two independent sets of samples were prepared and three Western blot analyses were performed of each set. Data are shown as mean ± SD. *p ≤ 0.05; **p ≤ 0.01; ***p ≤ 0.001.

applied at equitoxic concentrations, and after 24 h, the total RNA was extracted, reverse transcribed into cDNA, and used as a template in the PCR experiment. The relative fold changes were calculated by normalizing against the constitutively expressed housekeeping gene, glyceraldehyde-3-phosphate dehydrogenase (GAPDH). The upper panels in Figure 7 show that both enantiomers of **5b** decreased the mRNA levels for *c-myc* and *c-kit*. The levels of mRNA were reduced by ~30% at the highest concentrations (4 x IC_{50}) of **5b**.

In the next step, western blot analysis was carried out to examine the effect of **5b** on the translation of *c-MYC* and *c-KIT* (Figure 7C-E). The densitometric analysis of the gels in Figure 7C revealed that Λ-**5b** and Δ-**5b** at the highest concentration (4 x IC_{50}) reduced the c-myc protein levels by ~70%, and the c-kit protein levels by ~60% and ~40%, respectively.

These results, along with the results from qRT-PCR demonstrate that the enantiomers of **5b** were able to down-regulate the expression of *c-MYC* and *c-KIT* genes in human cells.

Discussion

The results show that the studied metallohelices bind with high affinity to G4 DNA while exhibiting much lower affinity towards duplex DNA. We consider that the remarkably strong and selective binding of these supramolecular architectures **5a**-**h** is part of a growing body of evidence that metallohelices, by nature of their similar shape, size, charge and amphipathic nature, emulate the properties of short peptidic α-helices.[21a]

The highest values of the binding affinity and selectivity towards G4 DNA were determined by the FID assay for **5b** and its *para* isomer **5a**. In addition, the binding selectivity of metallohelices was shown to be dependent on ionic strength. When the concentration of K^+ in the solution was raised from 40 to 110 mM, which is closer to the intracellular level (~140 mM), the binding affinities of most metallohelices towards G4 were lowered, but to a lesser extent than those to duplex DNA. As a result, selectivity indexes of the majority of metallohelices increased with the increase in ionic strength. The several-fold enhancement was observed for the enantiomers of **5a**,

5b, and a substantial increase was also registered for **5h**. For instance, the selectivity index of **5b** for *hTelo*, *c-myc*, *c-kit1*, and *c-kit2* G4s in 110 mM K^+ reached respectable values of 39, 62, 43, and 33 for the Δ-enantiomer and 7.8, 36, 23, and 17 for the Λ-enantiomer, respectively.

FRET melting assay demonstrated that **5a**-**h** stabilized DNA G4s even in the presence of excess amounts of dsDNA, which supports the binding preference of metallohelices towards G4 DNA over dsDNA. Consistent with the previous results, **5b** proved to be the most potent G4 stabilizer.

5a and **5b** were positively tested for their ability to inhibit primer elongation catalyzed by *Taq* DNA polymerase by stabilizing G4 structures formed in the template strands, with **5b** being slightly more efficient than **5a**. The highest inhibitory effect of **5a** and **5b** on the DNA synthesis was observed for the templates containing *c-myc* and *c-kit2* G4-forming sequences.

Based on the results of previous *in vitro* experiments, the influence of **5b** on the expression of *c-MYC* and *c-KIT* oncogenes in human embryonic kidney cells was explored, and both enantiomers of **5b** down-regulated *c-MYC* and *c-KIT* expression at mRNA and protein levels in a dose-dependent manner although the mRNA and protein levels did not perfectly correlate.

The binding mode of metallohelices to DNA G4s has not been elucidated. **5a**-**h** strongly interacted with four G4s that differ by their folding topologies and by the length and base composition of the connecting loops. Metallohelices, due to their size and shape, can either externally stack to the terminal G-quartets or bind to the grooves and loops, which could be a preferred binding mode since it does not require a flat aromatic structure. The experiments with 2Ap labeled *hTelo* G4, however, did not provide conclusive evidence that would favor one of the two potentially possible binding modes.

More information is needed to delineate a relationship between the overall size and shape of metallohelices and their G4 binding properties. Currently, it can only be concluded that shorter metallohelices **5b**, **5a**, and **5h** with Fe-Fe distances of 12.4 Å, 14 Å, and 14.4 Å, respectively, are generally better G4 binders than the remaining metallohelices **5c**-**g** with Fe-Fe distances longer than 17 Å.

We have recently demonstrated that metallohelices **5a**-**h** accumulate in eukaryotic cells and in the cell nucleus, where they interact with nucleic acids.[27] *In vitro* experiments revealed that metallohelices preferably bind to alternative nucleic acid structures, such as DNA[37] and RNA[38] bulges or human telomeric RNA G4.[39] Furthermore, metallohelices are efficient condensers of DNA molecules and can inhibit DNA-related enzymatic activities, including transcription and DNA relaxation.[27] Altogether, these results suggest that the biological activity of metallohelices is not characterized by a single specific mechanism but stems from the sum of several different contributions, including down-regulation of G4 DNA-mediated gene expression. Hence, metallohelices could, due to their ability to hit multiple targets, be considered multi-targeted agents.

Experimental Section

Chemicals and reagents. The metallohelices (Figure 1A) were synthesized according to previously published procedures.[26] Stability of the investigated metllohelices was studied by NMR and UV-vis.[26] The compounds are highly resistant to hydrolysis, with no noticeable decomposition over a period of weeks. Even in KCl/HCl buffer (pH 1.5) a $t_{1/2}$ of ca 11 days was measured for **5b**. Stock solutions of metallohelices were prepared in water at a concentration of 1 mM. The synthetic oligodeoxyribonucleotides were purchased from Eurofins Genomics (Ebersberg, Germany). T4 polynucleotide kinase and *Taq* DNA polymerase were from New England Biolabs (Beverly, MA). DNA from Micrococcus luteus and thiazole orange (TO) were from Sigma-Aldrich (Prague, Czech Republic). [γ-^{32}P]-ATP was purchased from Hartmann analytic GmbH (Braunschweig, Germany).

FID measurements. Oligonucleotides 22_*hTelo*, 5'-AGGGTTAGGGTTAGGGTTAGGG-3', 22_*c-kit1*, 5'-AGGGAGGGCGCTGGGAGGAGGG-3', 21_*c-kit2*, 5'-CGGGCGGGCGCGAGGGAGGGG-3', 22_*c-myc*, 5'-TGAGGGTGGGTAGGGTGGGTAA-3', and 26_ds 5'-CAATCGGATCGAATTCGATCCGATTG-3' were annealed at a 6.25 μM concentration in 10 mM potassium phosphate buffer (pH 7) and 30 or 100 mM KCl by heating to 95 °C for 5 min followed by slow cooling to room temperature and then stored in the refrigerator overnight. 10 mM stock solutions of thiazole orange (TO) were prepared in DMSO each week. Measurements were performed at 0.25 and 0.5 μM concentrations of oligonucleotides and TO, respectively, in a 0.5 cm quartz cuvette in a total volume of 0.6 mL. Small volumes (typically 1.2 μL) of metallohelices were added to the solution to obtain the desired concentration and thoroughly mixed by pipetting. Samples were left to equilibrate for 3 min at room temperature before data reading was taken. Measurements were carried out using Varian Cary Eclipse spectrofluorophotometer. The excitation and emission wavelengths were set to 501 nm and 538 nm, respectively, the excitation and emission slit widths were 10 nm, and the averaging time was set to 3 s.

FRET measurements. The double-labeled (donor fluorophore FAM, 6-carboxyfluorescein; acceptor fluorophore TAMRA, 6-carboxytetramethylrhodamine) oligonucleotides F21T_*hTelo*, 5'-FAM-GGGTTAGGGTTAGGGTTAGGG-TAMRA-3', F21T_*c-kit1*, 5'-FAM-GGGAGGGCGCTGGGAGGAGGG-TAMRA-3', F20T_*c-kit2*, 5'-FAM-GGGCGGGCGCGAGGGAGGGG-TAMRA-3', F21T_*c-myc*, 5'-FAM-GAGGGTGGGTAGGGTGGGTAA-TAMRA-3', and F26T_ds, 5'-FAM-CAATCGGATCGAATTCGATCCGATTG-TAMRA-3' were annealed at a 4 μM concentration in 10 mM potassium phosphate buffer (pH 7) by heating to 95 °C for 5 min followed by slow cooling to room temperature and then stored in the refrigerator overnight. Oligonucleotides at the concentration of 0.4 μM were mixed with 0.4 μM metallohelices in 4 mM potassium phosphate in the absence or presence of double-stranded (ds) DNA. Samples were prepared in 200 μL microtubes in a total volume of 40 μL. Measurements were performed on a real-time PCR instrument RotorGene 6000 (Corbett Research), with excitation at 470±10 nm and detection at 510±5 nm. The temperature was increased at a rate of 0.7 °C/min from 28 °C to 96 °C, and the fluorescence readings were taken at 1 min intervals. The melting temperatures (T_m) were calculated within the RotorGene 6000 application software by applying a first derivative calculation.

2-aminopurine (2Ap) fluorescence studies. The 2Ap-labeled oligonucleotides 22_*hTelo*_7-2Ap, 5'-AGGGTT*2Ap*GGGTTAGGGTTAGGG-3', 22_*hTelo*_13-2Ap, 5'-AGGGTTAGGGTT*2Ap*GGGTTAGGG-3', and 22_*hTelo*_19-2Ap, 5'-AGGGTTAGGGTTAGGGTT*2Ap*GGG-3' were annealed at a 40 μM concentration in 10 mM potassium phosphate (pH 7.0) and 30 mM KCl by heating to 95 °C for 5 min followed by slow cooling to room temperature and stored in the refrigerator overnight. A mixture of 4 μM oligonucleotide and 8 μM metallohelix was prepared in 10 mM potassium phosphate (pH 7.0) and 30 mM KCl in a total volume of 80 μL. Samples were placed in a quartz micro cuvette and left undisturbed at room temperature for 5 min before data readings were taken. Titrations of 2Ap-labeled 22_*hTelo* (1 μM final concentration) by metallohelices were performed in a 1 cm quartz cuvette in a total volume of 2.5 mL in 10 mM potassium phosphate (pH 7.0) and 30 mM KCl. Small volumes (2.5 μL) of metallohelices were added to the mixture to obtain the desired concentration and thoroughly mixed by pipetting. The samples were kept undisturbed for 3 min at room temperature before data readings were taken. The fluorescence was measured by using a Varian Cary Eclipse spectrofluorophotometer. The excitation and emission wavelengths were set to 310 nm and 365 nm, respectively, the excitation and emission slit widths were 10 nm, and the averaging time was set to 3 s.

DNA polymerase stop assay. This is a slightly modified assay described by Han and co-workers.[36a] Primer P22, 5'-TAATACGACTCACTATAGCAAT-3' (20 nM) was 5'-end-labeled with [γ-^{32}]ATP using T4 polynucleotide kinase and annealed to one of the complementary templates: *hTelo*_templ, 5'-TCCAACTATGTATACTTAGGGTTAGGGTTAGGGTTAGGGACATATCGATGAAATTGCTATAGTGAGTCGTATTA-3'; *c-myc*_templ, 5'-TCCAACTATGTATACTTTGAGGGTGGGTAGGGTGGGTAAACATATCGATGAAATTGCTATAGTGAGTCGTATTA-3'; *c-kit1*_templ, 5'-TCCAACTATGTATACTTAGGGAGGGCGCTGGGAGGAGGGACATATCGATGAAATTGCTATAGTGAGTCGTATTA-3'; *c-kit2*_templ, 5'-TCCAACTATGTATACTTCGGGCGGGCGCGAGGGAGGGGACATATCGATGAAATTGCTATAGTGAGTCGTATTA-3'; *c-myc*_templ_control, 5'-TCCAACTATGTATACTTTGAGCGTGCGTAGCGTGCGTAAACATATCG

ATGAAATTGCTATAGTGAGTCGTATTA-3'; *c-kit2*_templ_control, 5'-TCCAACTATGTATACTTCGCGCGCGCGAGCGAGCGGACATATCG ATGAAATTGCTATAGTGAGTCGTATTA-3' (30 nM) in 10 mM Tris-HCl (pH 8) buffer containing 25 mM KCl and 1.5 mM $MgCl_2$ by heating to 95 °C for 5 min followed by slow cooling to room temperature and then stored in the refrigerator overnight. Metallohelices at various concentrations were added to the samples (final volumes of 10 μL) and incubated at room temperature for 10 min. The primer extension reactions were initiated by adding dNTP (final concentration of 200 μM), and *Taq* DNA polymerase (4 units), and the samples were incubated for 60 min at 55 °C for *c-myc* and *c-kit2*, 45 °C for *c-kit1*, and 40 °C for *hTelo* G4 containing templates. The DNA synthesis was stopped by adding an equal volume of 2 × concentrated formamide loading buffer and heating to 90 °C for 3 min. DNA fragments were separated on a 12% PAA sequencing gel. Gels were exposed to a phosphor imaging plate and scanned with a GE Healthcare FLA 7000 laser scanner.

Cytotoxic/antiproliferative activity. HEK 293 (human embryonic kidney) cells were seeded at a density of 4 x 10^3 cells/well in 96-well plates in DMEM (high glucose 4.5 g.L^{-1}, supplemented with 50 μg.mL^{-1} gentamycin and 10% heat inactivated FBS) and grown overnight. The cells were treated with metallohelices at a series of concentrations (0 – 100 μM) for 72 hours. 10 μl MTT [3-(4,5-dimethyl-2-thiazolyl)-2,5-diphenyl-2*H*-tetrazolium bromide] was added (2.5 mg.mL^{-1} in PBS) and the cells were incubated for another 4 h. The medium was removed, and the insoluble formazan products were dissolved in DMSO. The absorbance at 570 nm vs. 620 nm was read using SPARK multimode plate reader (Tecan). The inhibition effect was expressed as IC_{50} values (concentration corresponding to 50% signal inhibition vs. control). The experiment was carried out in triplicate.

Real-time quantitative PCR. HEK 293 cells were seeded in 60 mm culture dishes at a density of 3 × 10^5 cells/dish and grown overnight in DMEM (high glucose 4.5 g.L^{-1}, supplemented with 50 μg.mL^{-1} gentamycin and 10% heat-inactivated FBS). Cells were treated with metallohelices for 24 h at various concentrations, and then, cells were harvested, washed, and pelleted. Cell pellets were immediately processed with RNeasy® Plus Mini Kit (QIAGEN), following the manufacturer´s instructions to obtain total RNA. One step RT-qPCR that combines reverse transcription followed by amplification thermal cycling was employed (Luna® universal one-step RT-qPCR (New England BioLabs, MA, USA)). Reactions were performed in Illumina Eco real-time PCR instrument (Illumina, CA, USA) with the following thermal profiles: 10 min at 55 °C (reverse transcription); 1 min at 95 °C (initial denaturation); 43 cycles of 10 s at 95 °C and 30 s at 60 °C (denaturation and extension, respective). The following primer sequences were used; GAPDH-F, 5'-GTCTCCTCTGACTTCAACAGCG-3', GAPDH-R, 5'-ACCACCCTGTTGCTGTAGCCAA-3', C-MYC-F, 5'-CCTGGTGCTCCATGAGGAGAC-3', C-MYC-R, 5'-CAGACTCTGACCTTTTGCCAGG-3', C-KIT-F, 5´-ATTGGTATTTTTGTCCAGGAACTGA-3´, C-KIT-R, 5´-TGGCCCAGATGAGTTTAGTGTCT-3´. Melting curve analysis and template-free negative controls were run to confirm specific single product amplification. GAPDH was used as the internal control. Relative mRNA expression is shown as fold increase ($2^{-\Delta\Delta Ct}$).[40]

Western blot analysis. HEK 293 cells were seeded in 60 mm culture dishes at a density of 3 × 10^5 cells/dish and grown overnight in DMEM medium (Dulbecco's Modified Eagle's Medium, high glucose 4.5 g L^{-1}, PAA, Pasching, Austria) supplemented with gentamycin (50 μg mL^{-1}, Serva) and 10% heat inactivated FBS; 37 °C, 5% CO_2 humidified atmosphere). Cells were treated with metallohelices for 24 h at various concentrations, and subsequently, cells were scraped, washed, pelleted, and lysed with ice cold RIPA buffer for one hour. Cellular extracts were cleared by centrifugation (15 000 rpm/10 min), mixed with 2 × LBS buffer (4% SDS; 10% 2-mercaptoethanol; 20% glycerol; 0. 004% bromophenol blue and 0.125 M Tris-HCl), and heated for 10 min at 95 °C. Proteins were separated on a 4-20% SDS-PAGE (Mini-PROTEAN® TGX™ Precast Gels), transferred to PVDF membrane, and detected using specific primary and secondary antibodies: Anti-GAPDH antibody, mouse monoclonal (Sigma-Aldrich; 1:200), Anti-c-Myc antibody [Y69] ab32072 (Abcam; 1:1000), Anti-c-Kit antibody [YR145] ab32363 (Abcam; 1:1000), Goat anti-Mouse IgG (H+L) Secondary antibody, HRP (ThermoFisher Scientific; 1:200) and Goat Anti-Rabbit IgG H&L (HRP) ab205718 (Abcam; 1:1000). SignalFire™ ECL Reagent (A+B) was used as a substrate, and the luminescence was visualized with Amersham Imager 680. Relative band intensities were determined by using Aida image analysis software.

Supporting Information

CD spectra of 22_*hTelo*, 22_*c-myc*, 22_*c-kit1*, and 21_*c-kit2* (Figure S1), displacement of thiazole orange from 22_*hTelo*, 22_*c-myc*, 21_*c-kit1*, 22_*c-kit2*, and 26_ds by Λ- and Δ-enantiomers of **5b** (Figure S2), DC_{50} values for 22_*hTelo*, 22_*c-myc*, 22_*c-kit1*, 21_*c-kit2* , and 26_ds determined by FID upon addition of metallohelices (Tables S1 and S3), binding selectivities of metallohelices towards 22_*hTelo*, 22_*c-myc*, 22_*c-kit1*, and 21_*c-kit2* (Tables S2 and S4), FRET melting curves (Figures S3-S7), fluorescence titrations of 22_*hTelo*_7-2Ap, 22_*hTelo*_13-2Ap, and 22_*hTelo*_19-2Ap with Λ- and Δ-enantiomers of **5b** and **5c** (Figure S8), inhibition of *Taq* polymerase DNA synthesis across template containing *c-myc*, *c-kit2*, *c-kit1*, and *hTelo* G4 forming sequences in the presence of increasing concentrations of **5a** (Figure S9), autoradiograms of sequencing gels with products of *Taq* polymerase DNA synthesis across *c-myc* control and *c-kit2* control templates in the presence of increasing concentrations of Λ-**5b** and Δ-**5b** (Figure S10).

Acknowledgements

This work was supported by the Czech Science Foundation [grant number 20-00735S].

Conflict of interest

The authors declare no conflict of interest.

Keywords: metalo-supramolecular helicates · DNA G-quadruplexes · oncogenes · multi-targeted agens

[1] J. Spiegel, S. Adhikari, S. Balasubramanian, *Trends Chem.* **2020**, *2*, 123-136.

[2] a) G. Biffi, D. Tannahill, J. McCafferty, S. Balasubramanian, *Nature Chem.* **2013**, *5*, 182; b) P. A. Summers, B. W. Lewis, J. Gonzalez-Garcia, R. M. Porreca, A. H. M. Lim, P. Cadinu, N. Martin-Pintado, D. J. Mann, J. B. Edel, J. B. Vannier, M. K. Kuimova, R. Vilar, *Nature Commun.* **2021**, *12*, 162.

[3] V. S. Chambers, G. Marsico, J. M. Boutell, M. Di Antonio, G. P. Smith, S. Balasubramanian, *Nature Biotechnol.* **2015**, *33*, 877-881.

[4] a) E. H. Blackburn, *Nature* **1991**, *350*, 569-573; b) J. L. Mergny, C. Helene, *Nature Med.* **1998**, *4*, 1366-1367.

[5] J. Dai, D. Chen, R. A. Jones, L. H. Hurley, D. Yang, *Nucleic Acids Res.* **2006**, *34*, 5133-5144.

[6] X. Tong, W. Lan, X. Zhang, H. Wu, M. Liu, C. Cao, *Nucleic Acids Res.* **2011**, *39*, 6753-6763.

[7] S. Cogoi, L. E. Xodo, *Nucleic Acids Res.* **2006**, *34*, 2536-2549.

[8] D. Y. Sun, K. X. Guo, J. J. Rusche, L. H. Hurley, *Nucleic Acids Res.* **2005**, *33*, 6070-6080.

[9] Y. Qin, E. M. Rezler, V. Gokhale, D. Sun, L. H. Hurley, *Nucleic Acids Res.* **2007**, *35*, 7698-7713.

[10] A. Siddiqui-Jain, C. L. Grand, D. J. Bearss, L. H. Hurley, *Proc. Natl. Acad. Sci. USA* **2002**, *99*, 11593-11598.

[11] S. Rankin, A. P. Reszka, J. Huppert, M. Zloh, G. N. Parkinson, A. K. Todd, S. Ladame, S. Balasubramanian, S. Neidle, *J. Am. Chem. Soc.* **2005**, *127*, 10584-10589.

[12] C. V. Dang, *Cell* **2012**, *149*, 22-35.

[13] a) W. Wang, S. Hu, Y. Gu, Y. Yan, D. B. Stovall, D. Li, G. Sui, *Biochim. Biophys. Acta - Rev. Cancer* **2020**, *1874*, 188410; b) B.-J. Chen, Y.-L. Wu, Y. Tanaka, W. Zhang, *Int. J. Mol. Sci.* **2014**, *10*, 1084-1096.

[14] M. Nannini, G. Biasco, A. Astolfi, M. A. Pantaleo, *J. Med. Genet.* **2013**, *50*, 653-661.
[15] X. Wang, C. X. Zhou, J. W. Yan, J. Q. Hou, S. B. Chen, T. M. Ou, L. Q. Gu, Z. S. Huang, J. H. Tan, *ACS Med. Chem. Lett.* **2013**, *4*, 909-914.
[16] Q. Li, J. F. Xiang, Q. F. Yang, H. X. Sun, A. J. Guan, Y. L. Tang, *Nucleic Acids Res.* **2013**, *41*, D1115-D1123.
[17] D. Monchaud, M. P. Teulade-Fichou, *Org. Biomol. Chem.* **2008**, *6*, 627-636.
[18] a) C. L. Ruehl, A. H. M. Lim, T. Kench, D. J. Mann, R. Vilar, *Chem. Eur. J.* **2019**, *25*, 9691-9700; b) O. Domarco, C. Kieler, C. Pirker, C. Dinhof, B. Englinger, J. M. Reisecker, G. Timelthaler, M. D. García, C. Peinador, B. K. Keppler, W. Berger, A. Terenzi, *Angew. Chem. Int. Ed.* **2019**, *58*, 8007-8012; *Angew. Chem.* **2019**, *131*, 8091-8096; c) M. Gillard, J. Weynand, H. Bonnet, F. Loiseau, A. Decottignies, J. Dejeu, E. Defrancq, B. Elias, *Chem. Eur. J.* **2020**, *26*, 13849-13860; d) J. Rubio-Magnieto, S. Kajouj, F. Di Meo, M. Fosséprè, P. Trouillas, P. Norman, M. Linares, C. Moucheron, M. Surin, *Chem. Eur. J.* **2018**, *24*, 15577-15588.
[19] S. K. Mishra, A. Tawani, A. Mishra, A. Kumar, *Sci. Rep.* **2016**, *6*, 38144.
[20] A. Minard, D. Morgan, F. Raguseo, A. Di Porzio, D. Liano, A. G. Jamieson, M. Di Antonio, *Chem. Commun.* **2020**, *56*, 8940-8943.
[21] a) H. Song, M. Postings, P. Scott, N. J. Rogers, *Chem. Sci.* **2021**, *12*, 1620-1631; b) M. J. Hannon, V. Moreno, M. J. Prieto, E. Moldrheim, E. Sletten, I. Meistermann, C. J. Isaac, K. J. Sanders, A. Rodger, *Angew. Chem. Intl. Ed.* **2001**, *40*, 879-884; *Angew. Chem.* **2001**, *113*, 903-908.
[22] a) H. Yu, X. Wang, M. Fu, J. Ren, X. Qu, *Nucleic Acids Res.* **2008**, *36*, 5695-5703; b) J. S. Wang, Y. Chen, J. S. Ren, C. Q. Zhao, X. G. Qu, *Nucleic Acids Res.* **2014**, *42*, 3792-3802.
[23] a) A. Zhao, S. E. Howson, C. Zhao, J. Ren, P. Scott, C. Wang, X. Qu, *Nucleic Acids Res.* **2017**, *45*, 5026-5035; b) C. Zhao, H. Song, P. Scott, A. Zhao, H. Tateishi-Karimata, N. Sugimoto, J. Ren, X. Qu, *Angew. Chem. Int. Ed.* **2018**, *57*, 15723-15727; *Angew. Chem.* **2018**, *130*, 15949-15953727.
[24] S. E. Howson, A. Bolhuis, V. Brabec, G. J. Clarkson, J. Malina, A. Rodger, P. Scott, *Nature Chem.* **2012**, *4*, 31-36.
[25] a) J. Malina, P. Scott, V. Brabec, *Dalton Trans.* **2015**, *44*, 14656-14665; b) V. Brabec, S. E. Howson, R. A. Kaner, R. M. Lord, J. Malina, R. M. Phillips, Q. M. A. Abdallah, P. C. McGowan, A. Rodger, P. Scott, *Chem. Sci.* **2013**, *4*, 4407-4416.
[26] D. H. Simpson, A. Hapeshi, N. J. Rogers, V. Brabec, G. J. Clarkson, D. J. Fox, O. Hrabina, G. L. Kay, A. K. King, J. Malina, A. D. Millard, J. Moat, D. I. Roper, H. Song, N. R. Waterfield, P. Scott, *Chem. Sci.* **2019**, *10*, 9708-9720.
[27] O. Hrabina, J. Malina, H. Kostrhunova, V. Novohradsky, J. Pracharova, N. Rogers, D. H. Simpson, P. Scott, V. Brabec, *Inorg. Chem.* **2020**, *59*, 3304−3311.
[28] D. Monchaud, C. Allain, M. P. Teulade-Fichou, *Bioorg. Med. Chem. Lett.* **2006**, *16*, 4842-4845.
[29] D. Renciuk, I. Kejnovska, P. Skolakova, K. Bednarova, J. Motlova, M. Vorlickova, *Nucleic Acids Res.* **2009**, *37*, 6625-6634.
[30] J. Kypr, I. Kejnovska, D. Renciuk, M. Vorlickova, *Nucleic Acids Res.* **2009**, *37*, 1713-1725.
[31] D. Monchaud, C. Allain, H. Bertrand, N. Smargiasso, F. Rosu, V. Gabelica, A. De Cian, J.-L. Mergny, M.-P. Teulade-Fichou, *Biochimie* **2008**, *90*, 1207-1223.
[32] J. L. Mergny, J. C. Maurizot, *ChemBioChem* **2001**, *2*, 124-132.
[33] T. Kimura, K. Kawai, M. Fujitsuka, T. Majima, *Tetrahedron* **2007**, *63*, 3585-3590.
[34] a) B. Holz, S. Klimasauskas, S. Serva, E. Weinhold, *Nucleic Acids Res.* **1998**, *26*, 1076-1083; b) E. L. Rachofsky, R. Osman and J. B. A. Ross, *Biochemistry* **2001**, *40*, 946-956.
[35] F. X. G. Han, R. T. Wheelhouse, L. H. Hurley, *J. Am. Chem. Soc.* **1999**, *121*, 3561-3570.
[36] a) H. Y. Han, L. H. Hurley, M. Salazar, *Nucleic Acids Res.* **1999**, *27*, 537-542; b) P. Wang, L. Ren, H. P. He, F. Liang, X. Zhou, Z. Tan, *ChemBioChem* **2006**, *7*, 1155-1159.
[37] O. Hrabina, J. Malina, P. Scott, V. Brabec, *Chem. Eur. J.* **2020**, *26*, 16554-16562.
[38] J. Malina, P. Scott, V. Brabec, *Chem. Eur. J.* **2020**, *26*, 8435-8442.
[39] J. Malina, P. Scott, V. Brabec, *Sci. Rep.* **2020**, *10*, 14543.
[40] K. J. Livak, T. D. Schmittgen, *Methods* **2001**, *25*, 402-408.

10.1002/chem.202101388

Entry for the Table of Contents

FULL PAPER

DNA G-quadruplexes (G4s) represent attractive targets for cancer therapy. We show that the metallohelices, which exhibit bioactivity emulating the natural systems, bind with high affinity to G4 DNA and inhibit activity of DNA polymerase by stabilizing G4 structures. Moreover, the investigated metallohelices down-regulate the expression oncogenes in human embryonic kidney cells at mRNA and protein levels holding promise as potential multi-targeted drugs.

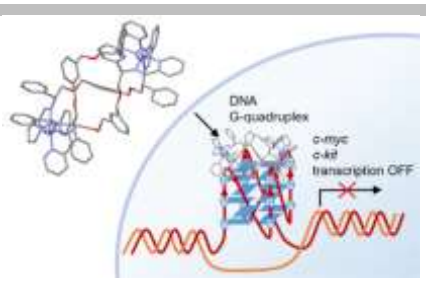

Jaroslav Malina, Hana Kostrhunova, Peter Scott and Viktor Brabec*

Page No. – Page No.

Fe(II) Metallohelices Stabilize DNA G-Quadruplexes and Down-regulate Expression of G-Quadruplex Regulated Oncogenes